Journal of Advanced Joining Processes 9 (2024) 100175

Contents lists available at ScienceDirect

Journal of Advanced Joining Processes

journal homepage: www.sciencedirect.com/journal/journal-of-advanced-joining-processes

Multi-planar injection lap riveting

Miguel S.T. Sapage [a], João P.M. Pragana [a], Rui F.V. Sampaio [a], Ivo M.F. Bragança [a,b], Carlos M. A. Silva [a], Paulo A.F. Martins [a,*]

[a] IDMEC, Instituto Superior Técnico, Universidade de Lisboa, Portugal
[b] CIMOSM, Instituto Superior de Engenharia de Lisboa, Instituto Politécnico de Lisboa, Portugal

ARTICLE INFO

Keywords:
Multi-planar hybrid busbars
Injection lap riveting
Finite element modelling
Experimentation

ABSTRACT

This paper is focused on multi-planar hybrid busbars made from copper and aluminum for electric energy distribution systems. The objective is to provide an overview of its assembly by injection lap riveting in multidirectional tools and to compare the electrical performance of its joints against that of conventional (in-plane) busbars.

The injected lap riveted joints require a dovetail ring hole and a countersunk hole to be first machined in the overlapped copper and aluminum sheets and then to inject the semi-tubular rivets by compression through the lined-up holes in order to fix the sheets in position. In this work, the injection of the semi-tubular rivets was carried out in a laboratory multidirectional tool set that converts the vertical press stroke into two-orthogonal horizontal movements by means of cam slide units consisting of compression punch holders and sliding wedge actuators attached to the upper bolster.

Experimental results obtained for a multi-planar, three-conductor, rake-shaped elbow of a hybrid busbar system allow concluding that while the required compression force is proportional to the number of injected lap riveted joints, the electrical performance is non-proportional due to changes in the distribution of electric current density. Numerical simulation with finite elements gives support to the discussion and allows readers to recognize the pitfalls of designing busbar joints exclusively based on mechanical requirements.

Introduction

Injection lap riveting (ILR) is a mechanical joining process originally proposed by Ferreira et al. (2021) to connect two sheets made from similar or dissimilar materials placed one on top of the other, at ambient temperature. The process belongs to the sub-category of joining by plastic deformation with auxiliary external elements (Meschut et al., 2022) (Fig. 1a) and requires first to machine a dovetail ring hole and a countersunk hole in the lower and upper sheets, respectively, and then to inject a semi tubular rivet by compression through the lined-up holes to create a mechanical interlocking that fixes the two sheets in position (Fig. 1b).

The development and applications of ILR have been mainly focused on the fabrication of lap joints for monolithic and hybrid (copper-aluminum) busbars for electric energy distribution systems due to the possibility that the process offers of being used in situ and generating high contact pressures along the interfaces between the sheets and the rivets (Pragana et al., 2022; Sampaio et al., 2023).

Compared to other processes included in the sub-category of joining by plastic deformation with auxiliary elements (Fig. 1a), it can be said that self-pierce riveting (SPR) may also be applied to produce lap joints in hybrid busbars with savings in the overall manufacturing time because it does not require punching or machining of holes (Li et al., 2017). However, the performance of self-pierced riveted joints in electrical applications is poorer than that of injection lap riveted joints due to the disturbances in electric current flow caused by the high electric resistivity of the steel rivets that are driven through the sheets and to the material protrusions that are plastically formed above and below the sheet surfaces.

In the case of clinching, included in the sub-category of joining by plastic deformation without auxiliary elements (Fig. 1a), the electrical resistance of the lap joints is expected to further increase due to disturbances in the electric current flow caused by the hole left by the punch, by material protrusions, and by severe local plastic deformation of the sheet materials (Jiang et al., 2015). Large dislocation pile-up and grain distortion induced by the clinching process as well as the

* Corresponding author.
E-mail address: pmartins@tecnico.ulisboa.pt (P.A.F. Martins).

https://doi.org/10.1016/j.jajp.2023.100175

Available online 7 December 2023

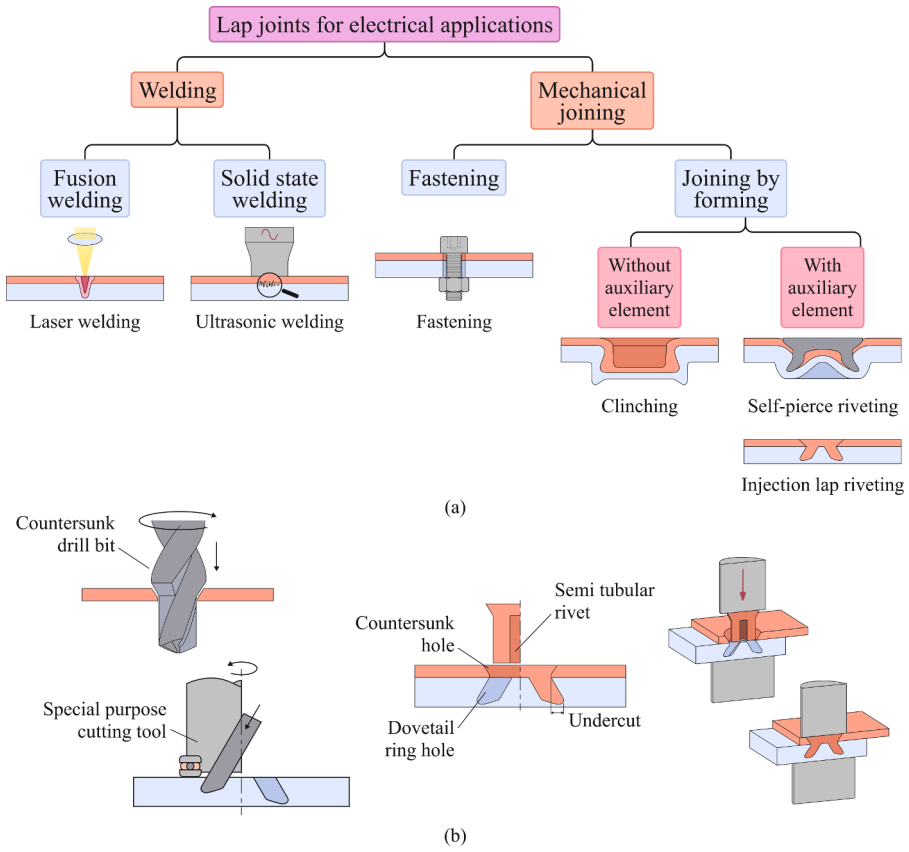

Fig. 1. (a) Classification of the main joining technologies to fabricate lap joints for electrical applications with examples of typical processes. (b) Schematic representation of the machining and injection by compression stages of the injection lap riveting process.

imperfections in crystal structure have a negative influence in the electric performance of the joint materials (Karolik and Luhvich, 1994). In addition to what was said, it is worth noticing that clinching is limited to small sheet thicknesses and that it requires the harder sheets to be placed on the punch side (Chen et al., 2021).

Regarding the differences between ILR and fastening (Fig. 1a), it can be said that the latter is the most used process in the fabrication of lap joints for busbars in electric energy distribution systems (Lee et al., 2010). However, the use of bolts and nuts gives rise to non-uniform local contact pressures on the sheet surfaces that create disturbances in the electric current flow (Park and Cho, 2014; Tzeneva et al., 2007) and significant increases in electrical resistance in the case of unintentional loosening of the fasteners (Sampaio et al., 2022b).

In what concerns the comparison between ILR and welding processes (Fig. 1a), it can be said that although the number of welding processes is large, their application to the fabrication of lap joints made from dissimilar materials (like the copper-aluminum joints of hybrid busbars) suffers from multiple problems related to the metallurgical changes, residual stresses and distortions induced by the heat-cooling cycles (Brandon and Kaplan, 1997; Sadeghian and Iqbal, 2022). These problems are responsible for degradation in quality, accuracy, and reliability of the lap joints, and often limit their applicability to monolithic busbar systems (i.e., to busbar systems made from a single or similar materials).

Despite the technical, economic, and environmental advantages of ILR over the existing joining processes for the fabrication of lap joints in hybrid busbar systems (Pragana et al., 2023), investigations have mainly been focused on conventional (in-plane) joints. No attention has so far been paid to the fabrication methods and electric performance of joints

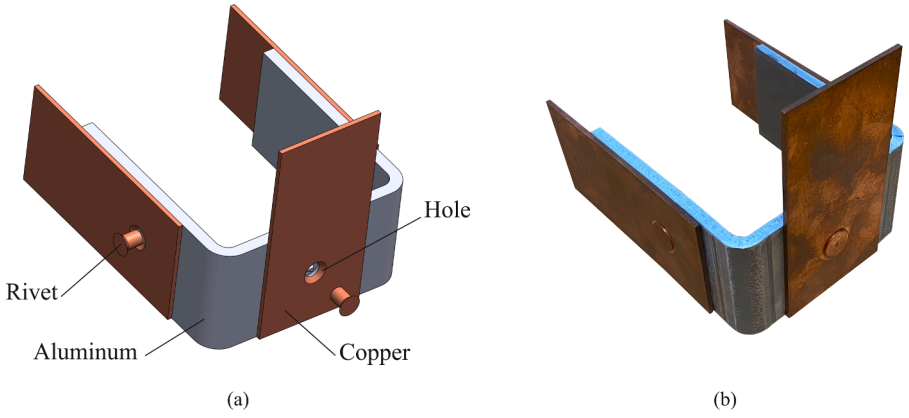

Fig. 2. (a) Scheme with notation and (b) photograph of the three-conductor rake-shaped elbow fabricated by injection lap riveting.

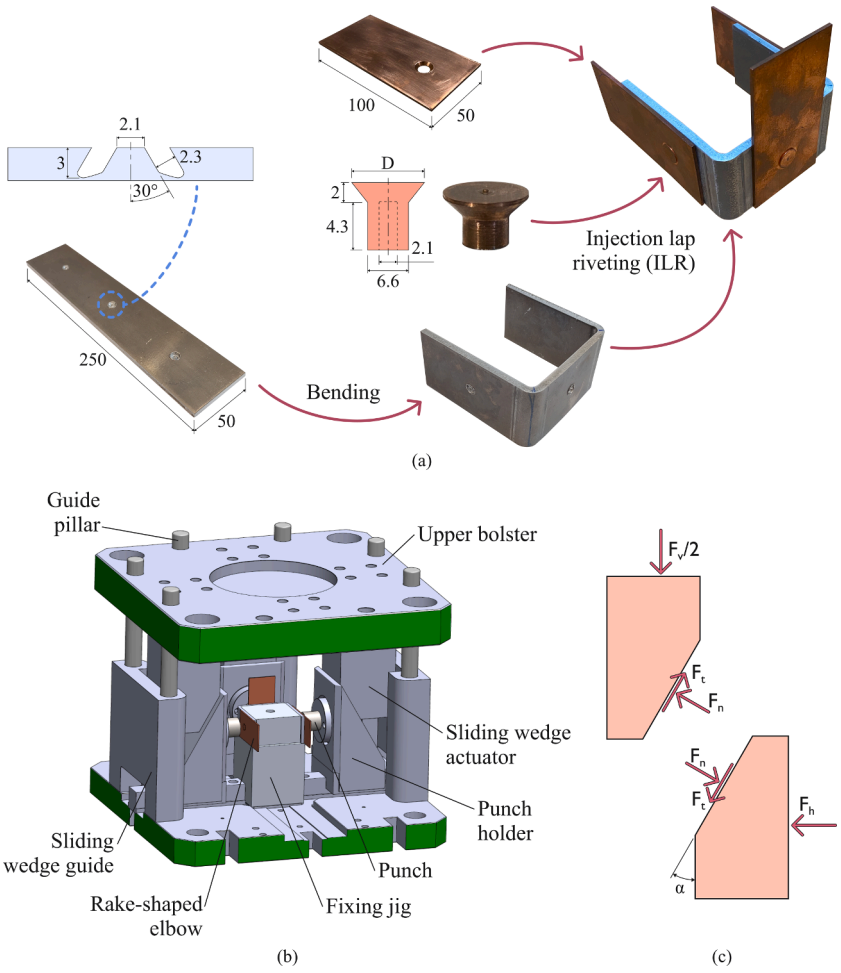

Fig. 3. (a) Fabrication sequence of the rake-shaped elbows made from copper and aluminum sheets, (b) schematic representation of multiple injection lap riveting operations carried out simultaneously in a multidirectional tool and (c) detail of the free-body diagram of the cam slide units.

in multi-planar hybrid busbar systems.

Under these circumstances, this paper is focused on multi-planar hybrid busbars made from copper and aluminum with a twofold objective: (a) to discuss the assembly of a three-conductor rake-shaped elbow (Fig. 2) by injection lap riveting in a multidirectional tool and (b) to compare its electrical performance in direct current (DC) conditions with that of an ideal rake-shaped elbow and a conventional (in-plane) joint to highlight the importance of combining both mechanical and electrical requirements in the design of multi-planar hybrid busbar joints.

Methods and procedures

Materials and mechanical characterization

The rake-shaped elbows were fabricated from aluminum AA6082-T6 sheets with $t_{Al} = 5$ mm thickness and electrolytic copper C11000 sheets with $t_{Cu} = 2$ mm thickness, to obtain a ratio $t_{Al}/t_{Cu} = 2.5$ close to the theoretical value of 2.3 that ensures equal electrical conductance in both sheets (Sampaio et al., 2022a). The rivets with 5 mm radius were machined from electrolytic copper C11000 rods with 15 mm diameter.

The mechanical characterization of the aluminum sheets was carried out in an Instron 4507 universal testing machine by means of tensile specimens that were extracted from the sheets and tested in accordance with the ASTM standards E8/E8M (2016). The mechanical characterization of the copper rods was carried out in the same testing machine by means of compression specimens in accordance with the ASTM standards E9-89A (2000). The true stress vs. true strain responses at ambient temperature resulting from the mechanical characterization tests performed in both materials were approximated by the following Holloman strain hardening models,

$$\text{Copper C11000}: \ \sigma = 339\,\varepsilon^{0.002}\ \text{(MPa)} \tag{1}$$

$$\text{Aluminium AA6082} - \text{T6}: \ \sigma = 381\,\varepsilon^{0.08}\ \text{(MPa)} \tag{2}$$

Fabrication of the rake-shaped elbows

Fabrication of the rake-shaped elbows involved three main stages (Fig. 3a). Firstly, the dovetail ring holes, and countersunk holes were machined in the aluminum and copper sheets using a flexible cutting tool recently developed by the authors (Pragana et al., 2024) and a conventional drilling machine equipped with a countersunk drill bit. Then, the aluminum sheets were locally heated and bent at a 90-degree angle with an inner radius $r_i \cong 5$ mm. Finally, the copper and aluminum sheets were assembled into the rake-shaped elbows by means of injection lap riveting.

The final stage is shown in Fig. 3b, in which the copper and aluminum sheets are placed in position using a fixing jig with a wall recess around its perimeter. The semi-tubular copper rivets, placed in-between the machined holes of the copper and aluminum sheets, allow fine tuning the positioning while ensuring concentricity of the holes. The semi-tubular rivets are then injected by compression, simultaneously, to assemble the rake-shaped elbow.

The tool was installed in an Instron SATEC 1200 kN hydraulic testing

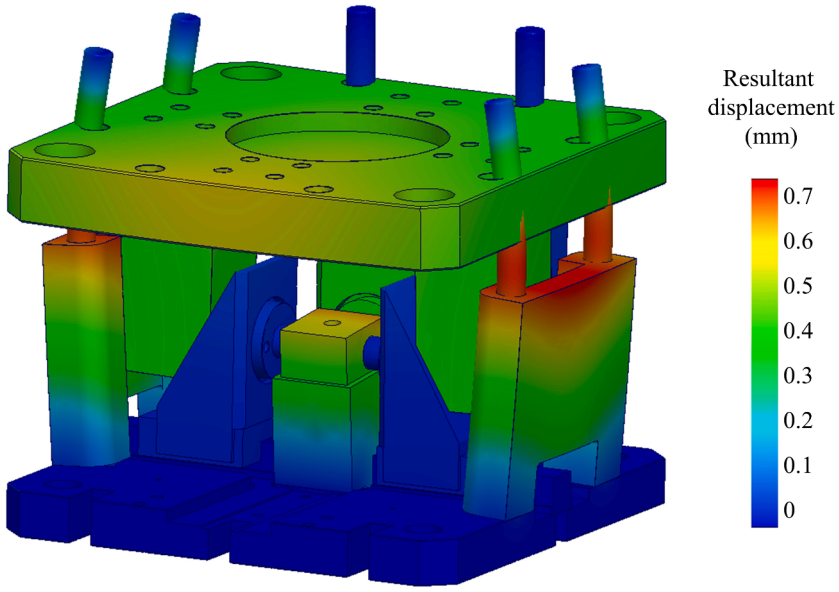

Fig. 4. Magnified deformation (25 ×) of the multidirectional tool under a vertical compression force of 200 kN obtained by finite element analysis.

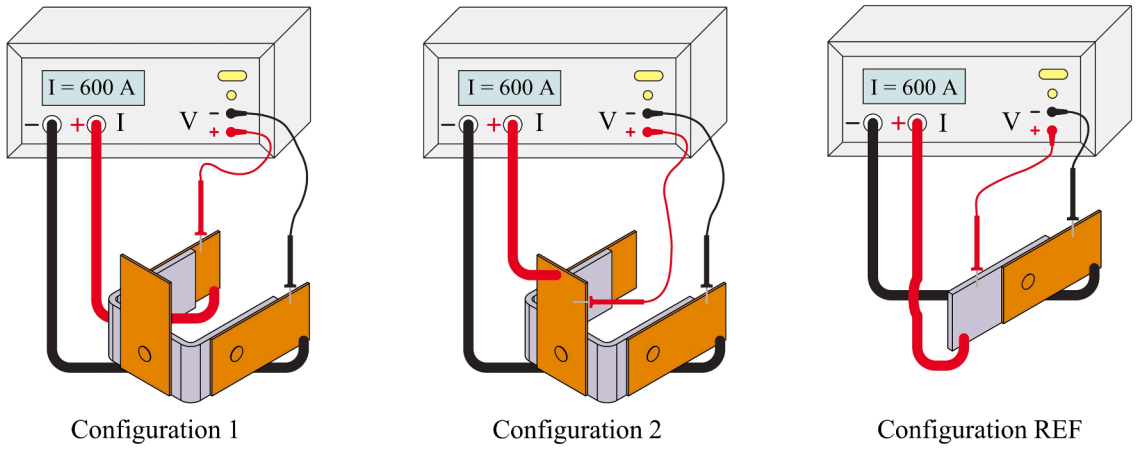

Fig. 5. The two different configurations (1 and 2) for measuring the electrical resistance of the rake-shaped elbow plus the reference configuration (REF) consisting of a conventional (in-plane) hybrid joint.

machine and the tests were carried out with a constant crosshead speed of 5 mm/min.

The free-body diagram included in Fig. 3c shows the conversion of the vertical press force F_v into one of the two-orthogonal horizontal forces F_h by means of cam slide units with a working angle α consisting of compression punch holders and sliding wedge actuators attached to the upper bolster. The force equilibrium along the vertical v and horizontal h directions of each pair of cam slide units provides the following relation,

$$\begin{aligned} &\text{Vertical direction}: \ \frac{1}{2}F_v = F_n(\sin\alpha + \mu\cos\alpha) \\ &\text{Horizontal direction}: \ F_h = F_n(\cos\alpha - \mu\sin\alpha) \end{aligned} \tag{3}$$

where $F_t = \mu F_n$ is the friction force, μ is the friction coefficient along the contact surfaces of the cam slide units and F_n is the normal force to these surfaces. Combination of the two above equations (3) allows writing the horizontal force F_h in each orthogonal direction as a function of the vertical tool force F_v, as follows,

$$F_h = F_v \frac{\cos\alpha - \mu\sin\alpha}{2(\sin\alpha + \mu\cos\alpha)} \tag{4}$$

In the multidirectional tool utilized in the experiments, the working angle of the cam slide units $\alpha = 30^{\circ}$

The guided pillars prevent excessive deformation of the sliding wedge guides under loading whilst ensuring the alignment between the upper and lower tool halves. Fig. 4 shows the magnified deformation of the tool (25 ×) under a vertical compression force of 200 kN obtained by finite element analysis in SolidWorks, in which it is possible to observe the role played by the guided pillars in minimizing excessive deformation of the sliding wedge guides.

Electrical characterization of the rake-shaped elbows

The electrical characterization of the rake-shaped elbow consisted in determining its electrical resistance at ambient temperature using two different measuring configurations (Fig. 5). Configuration 1 corresponds to the U-flatwise part and configuration 2 to the L-twisted part of the rake-shaped elbow.

Determination of the electrical resistance for each measuring configuration employed a four-point probe technique (Kumar et al., 2021) that made use of two probes placed some distance apart and connected to a KoCoS PROMET R600 micro-ohmmeter. The latter

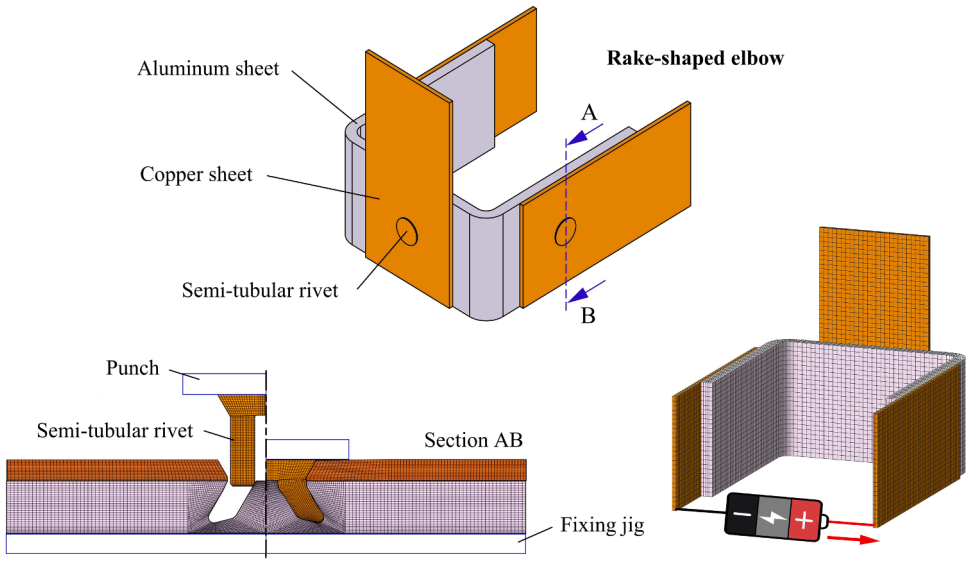

Fig. 6. (a) Two-dimensional model of the injection lap riveting of a typical hybrid joint (before and after assembly) and (b) three-dimensional model of the entire rake-shaped elbow to simulate the electric current flow and determine the electrical resistance (the DC circuit shown in the figure corresponds to configuration 1 of Fig. 5).

supplied an electric current of 600 A (DC) for approximately 2 s to measure the drop in voltage and calculate the electrical resistance of the rake-shaped elbow by Ohm's law.

Further details on the experimental setup and measuring procedures are given by Sampaio et al. (2022a), who also provide information on the electric resistivities of the copper ρ^{e}_{Cu} = 17.64 μΩ.mm and aluminium ρ^{e}_{Al} = 40.58 μΩ.mm sheets at ambient temperature. These values will be used in the finite element modelling of the electric current flow across the rake-shaped elbow.

The electrical resistance of a conventional (in-plane) hybrid joint was also measured for comparison purposes (refer to 'Configuration REF' in Fig. 5).

Finite element modelling

Injection lap riveting was simulated with the in-house finite element computer software i-form (Nielsen and Martins, 2021) assuming that plastic deformation of the semi-tubular rivets and neighboring materials was rotational symmetric (two-dimensional). The punches and fixing jigs were considered as rigid contact-friction objects (Fig. 6a).

The flow of electric current across the rake-shaped elbow was simulated with the electrical module of the above-mentioned finite element computer software. Three-dimensional meshes making use of hexahedral elements needed to be used because rotational symmetric conditions are not applicable to the electrical analysis (Fig. 6b). The models did not account for the influence of temperature because the busbars were tested at ambient temperature and because the temperature rise during the very short time duration of each measurement performed with the micro-ohmmeter was negligible (below 1 °C).

Electrical finite element simulations were carried out for ideal rake-shaped elbows without rivets, in which all the adjacent sheets are in perfect contact and without contaminant or oxide films along their interfaces. The simulations performed under these modelling conditions provided the minimum electrical resistance values that will be used in the following sections of the paper for comparison and normalization purposes.

The mechanical and electrical data for performing the finite element simulations were retrieved from previous sections 2.1 and 2.3.

Results and discussion

Injection lap riveting forces

The friction coefficient μ to be used in the analytical conversion (3) between the horizontal force F_h acting in a specific direction and the vertical tool force F_v measured by the load cell of the hydraulic testing machine was determined by compressing cylindrical specimens between straight parallel compression punches. The tests involved single-action vertical tool movements, when the punch holders were fixed to the upper and lower bolsters, and conversion of the vertical press stroke into

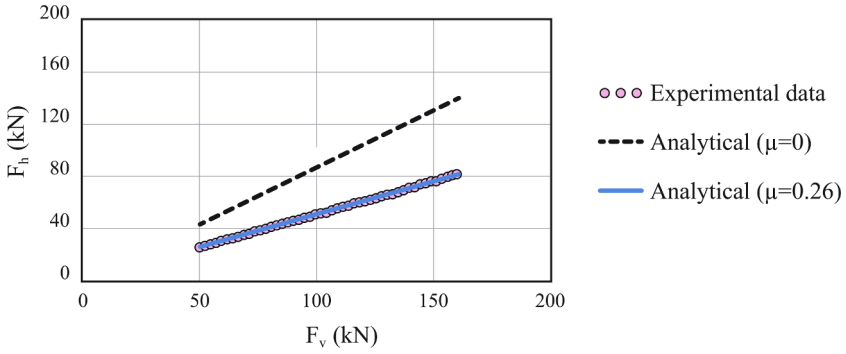

Fig. 7. Analytical (3) and experimental conversions between the horizontal F_h and vertical F_v forces for double-acting cam slide units moving along each specific horizontal direction.

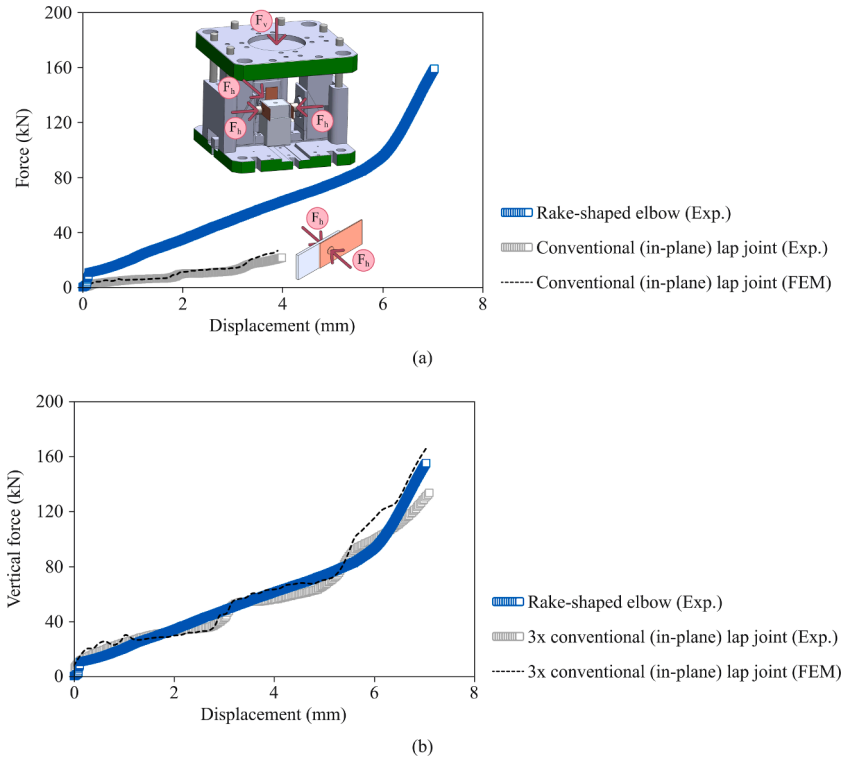

Fig. 8. (a) Experimental evolution of the vertical force with vertical displacement $F_v(v)$ to fabricate the three-injection lap riveted joints of the rake-shape elbow simultaneously and the experimental and finite element computed evolutions of the horizontal force with horizontal displacement $F_h(h)$ to fabricate a single conventional (in-plane) lap joint. (b) Modification of (a) after correcting the force vs. displacement evolution of the conventional (in-plane) lap joint into vertical direction and accounting for the total number of joints.

horizontal movements, when the punch holders were fixed to the cam slide units. In the case of the latter, tests were carried out in each orthogonal horizontal direction at a time.

The results of these tests are shown in Fig. 7 and allow concluding that the analytical conversion given by Eq. (3) and the experimental values coincide for a linear relationship with a slope of 0.508 when the friction coefficient $\mu = 0.26$,

$$F_h = 0.508F_v \text{ for } \mu = 0.26 \tag{5}$$

The conversion between the horizontal F_h and vertical F_v tool forces allow understanding the results illustrated in Fig. 8a and b. Fig. 8a provides the experimental evolution of the vertical force with vertical displacement $F_v(v)$ to fabricate the three-injection lap riveted joints of the rake-shaped elbow, simultaneously, along the two-orthogonal horizontal directions (refer to the blue open rectangles).

The other two evolutions in Fig. 8a correspond to the experimental and finite element computed evolution of the horizontal force with horizontal displacement $F_h(h)$ during injection lap riveting of a conventional (in-plane) lap joint. The agreement between experimental and finite element evolutions is very good but the extrapolation of these

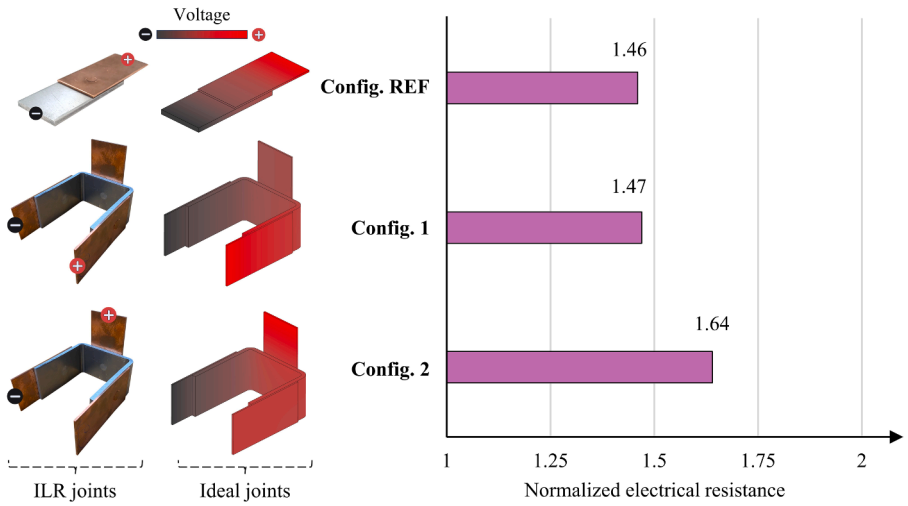

Fig. 9. Normalized electrical resistance for three different measuring configurations in which the reference configuration (REF) corresponds to a conventional (in-plane) hybrid lap joint. The values were calculated by dividing the experimental electrical resistance of each configuration obtained by injection lap riveting (ILR) by its ideal electrical resistance determined by finite element analysis.

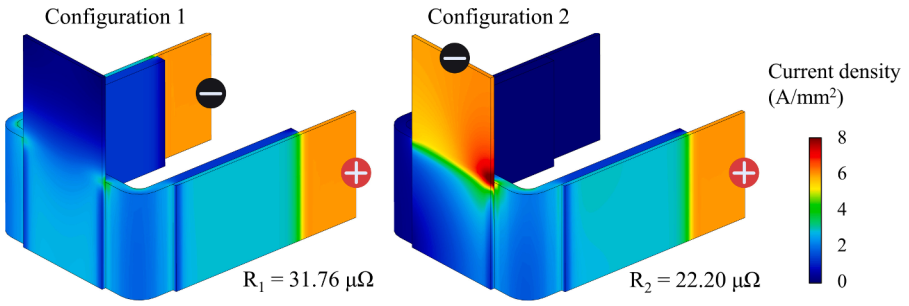

Fig. 10. Finite element predicted distribution of current density (A/mm2) for the measuring configurations 1 and 2 of Fig. 5.

results into vertical direction $F_v(v)$ required accounting for the total number of joints in the rake-shaped elbow, the conversion (5) between horizontal F_h and vertical F_v forces, and the following relation between the horizontal h and vertical v displacements of the cam slide units,

$$h = v\tan\alpha \tag{6}$$

All this combined in the fabrication of the three-injection lap riveted joints of the rake-shape elbow allows plotting the $F_v(v)$ evolutions that are shown in Fig. 8b, which prove that superposition applies to the injection lap riveting force vs. displacement evolutions in multidirectional tools. As seen, the experimental force-displacement evolution of the riveting process to fabricate the rake-shaped elbow is monotonic and smooth, while those obtained by extrapolation of the experimental and finite element results for a conventional (in-plane) lap joint show oscillation. This is attributed to minor geometrical and positioning variations of the rivets and sheets used in the rake-shaped elbow, which are responsible for the riveting process not being carried out at the same precise instant of time for the three rivets.

Electrical performance

Fig. 9 contains normalized values of the electrical resistance for the different measuring configurations illustrated in Fig. 5. The normalization was built upon the ratio between the experimental and the ideal electrical resistances in which the former is measured in accordance with the procedure described in section 2.3 and the latter is calculated by finite elements assuming perfect contact, without contaminant or oxide films along the sheet interfaces.

This methodology allows comparing the electrical resistance of each measuring configuration without the influence of length, width and overlap area, which give rise to different absolute electrical resistance values and could induce erroneous interpretations of their relative performances.

As seen in Fig. 9, the normalized electrical resistance of the rake-shaped elbow measured with configuration 1 is almost identical to that of a conventional (in-plane) hybrid lap joint (reference configuration). In contrast, the normalized electrical resistance of the rake-shaped elbow measured with configuration 2 is 12 % greater than that of configuration 1.

This result allows concluding that electric current flows more easily across the U-flatwise part than across the L-twisted part of the rake-shaped elbow. Further evidence of this is given by the finite element computed distribution of current density depicted in Fig. 10, in which the highest values are located on the right side of the vertical connector due to a greater disruption of the electric current flow at the corner.

Finally, it is worth mentioning that the highest electrical resistance of configuration 1 (31.76 μΩ) is due to a larger distance between the measuring probes than in configuration 2. This was the reason why the differences in electrical performance that are disclosed in Fig. 9 made use of normalized values built upon the ratio between the experimental and the ideal electrical resistances of the different configurations. Otherwise, one could be led to wrongly conclude that electric current flow in configuration 2 was the best.

Conclusions

A multi-planar hybrid busbar connector consisting of a three-conductor rake-shaped elbow was successfully assembled in a single press stroke using a multidirectional tool set. The total force required by the press was determined through the conversion of the force vs. displacement evolutions of conventional (in-plane) joints from horizontal to vertical direction taking into consideration the working angle and coefficient of friction of the cam sliding units, and the total number of rivets that are driven into the dovetail ring holes, simultaneously. Results show that superposition applies to the injection lap riveting force vs. displacement evolutions in multidirectional tools.

In contrast, measurements of electrical resistance along two different configurations corresponding to the U-flatwise and the L-twisted parts of the rake-shaped elbow demonstrate the breakdown of symmetry and superposition due to easier electric current flow across the U-flatwise part. This is further confirmed by the finite element predicted distributions of current density.

In a broader sense, what results seem to indicate is that the advantage of using symmetrical geometries to make the preparation and fabrication of the joints easier must be duly weighted with the electrical efficiency to improve the overall design of the injection lap riveted joints.

CRediT authorship contribution statement

Miguel S.T. Sapage: Data curation, Investigation, Software. **João P. M. Pragana:** Conceptualization, Data curation, Investigation, Methodology, Software, Supervision, Validation, Visualization, Writing – review & editing. **Rui F.V. Sampaio:** Data curation, Investigation, Methodology, Software, Validation, Writing – review & editing. **Ivo M. F. Bragança:** Conceptualization, Data curation, Investigation, Methodology, Supervision, Validation, Visualization, Writing – review & editing. **Carlos M.A. Silva:** Conceptualization, Data curation, Investigation, Methodology, Software, Supervision, Validation, Visualization, Writing – review & editing. **Paulo A.F. Martins:** Conceptualization, Funding acquisition, Investigation, Project administration, Resources, Validation, Writing – original draft, Writing – review & editing.

Declaration of Competing Interest

The authors declare that they have no known competing financial interests or personal relationships that could have appeared to influence the work reported in this paper.

Data availability

Data will be made available on request.

Acknowledgements

The authors would like to acknowledge the support provided by Fundação para a Ciência e a Tecnologia of Portugal and IDMEC under LAETA- UIDB/50022/2020 and PTDC/EME-EME/0949/2020. Rui Sampaio would also like to acknowledge the support under the PhD Studentship 2022.12351.BD.

References

ASTM E8/E8 M, 2016. Standard Test Methods For Tension Testing of Metallic Materials. ASTM International, West Conshohocken, USA.

ASTM E9-89A, 2000. Standard Test Methods of Compression Testing of Metallic Materials At Room Temperature. ASTM International, West Conshohocken, USA.

Brandon, D., Kaplan, W.D., 1997. Joining Processes: an Introduction. John Wiley & Sons, Chichester, UK.

Chen, C., Zhang, H., Zhao, S., Ren, X., 2021. Effects of sheet thickness and material on the mechanical properties of flat clinched joint. Front. Mech. Eng. 16, 410–419.

Ferreira, F.R., Pragana, J.P.M., Bragança, I.M.F., Silva, C.M.A., Martins, P.A.F., 2021. Injection lap riveting. CIRP Ann. – Manuf. Technol. 70, 261–264.

Jiang, T., Liu, Z.X., Wang, P.C., 2015. Effect of aluminum pre-straining on strength of clinched galvanized SAE1004 steel-to-AA6111-T4 aluminum. J. Mater. Process. Technol. 215, 193–204.

Karolik, A.S., Luhvich, A.A., 1994. Calculation of electrical resistivity produced by dislocations and grain boundaries in metals. J. Phys.: Condens. Matter 6, 873–886.

Kumar, N., Masters, I., Das, A., 2021. In-depth evaluation of laser-welded similar and dissimilar material tab-to-busbar electrical interconnects for electric vehicle battery pack. J. Manuf. Process. 70, 78–96.

Lee, S.S., Kim, T.H., Hu, S.J., Cai, W., 2010. Joining technologies for automotive lithium-ion battery manufacturing: a review. In: ASME 2010 International Manufacturing Science and Engineering Conference, Pennsylvania, USA, 1, pp. 541–549.

Li, D., Chrysanthou, A., Patel, I., Williams, G., 2017. Self-piercing riveting - a review. Int. J. Adv. Manuf. Technol. 92, 1777–1824.

Meschut, G., Merklein, M., Brosius, A., Drummer, D., Fratini, L., Füssel, U., Gude, M., Homberg, W., Martins, P.A.F., Bobbert, M., Lechner, M., Kupferf, R., Groger, B., Han, D., Kalich, J., Kappe, F., Kleffel, T., Kohler, D., Kuball, C.M., Popp, J., Romisch, D., Troschitz, J., Wischer, C., Wituschek, S., Wolf, M., 2022. Review on mechanical joining by plastic deformation. J. Adv. Join. Process. 5, 100113.

Nielsen, C.V., Martins, P.A.F., 2021. Finite element flow formulation. Metal Forming: Formability, Simulation and Tool Design. Academic Press, London, UK, pp. 181–249.

Park, S.W., Cho, H., 2014. A practical study on electrical contact resistance and temperature rise at the connections of the copper busbars in switchgears. In: IEEE 60th Holm Conference on Electrical Contacts, New Orleans, USA, pp. 1–7.

Pragana, J.P.M., Sampaio, R.F.V., Bragança, I.M.F., Silva, C.M.A., Martins, P.A.F., 2022. Injection lap riveting of aluminum busbars – a thermo-electro-mechanical investigation. J. Manuf. Mater. Process. 6, 74.

Pragana, J.P.M., Sampaio, R.F.V., Bragança, I.M.F., Silva, C.M.A., Martins, P.A.F., 2024. An injection lap riveting tool system. In: Proceedings of The 14th International Conference on the Technology of Plasticity ICTP 2023 (Eds. Mocellin K., Bouchard P. O., Bigot R., Balan T.), Mandelieu - La Napoule, France, Spinger Nature, Switzerland, 3: 81–90.

Pragana, J.P.M., Sapage, M.S.T., Sampaio, R.F.V., Bragança, I.M.F., Ribeiro, I., Silva, C. M.A., Martins, P.A.F., 2023. Joining of hybrid busbars for E-mobility: an economic and environmental study. J. Adv. Join. Process. 8, 100159.

Sadeghian, A., Iqbal, N., 2022. A review on dissimilar laser welding of steel-copper, steel-aluminum, aluminum-copper, and steel-nickel for electric vehicle battery manufacturing. Optics Laser Technol. 146, 107595.

Sampaio, R.F.V., Pragana, J.P.M., Bragança, I.M.F., Silva, C.M.A., Martins, P.A.F., 2023. Thermo-electrical performance of hybrid busbars: an experimental and numerical investigation. J. Mater.: Des. Appl. 237, 70–80.

Sampaio, R.F.V., Pragana, J.P.M., Bragança, I.M.F., Silva, C.M.A., Nielsen, C.V., Martins, P.A.F., 2022b. Electric performance of fastened hybrid busbars: an experimental and numerical study. J. Mater.: Des. Appl. 263, 1152–1163.

Sampaio, R.F.V., Pragana, J.P.M., Clara, R.G., Bragança, I.M.F., Martins, P.A.F., 2022a. New self-clinching fasteners for electric conductive connections. J. Manuf. Mater. Process. 6, 159.

Tzeneva, R., Slavtchev, Y., Mladenov, V., 2007. New connection design of high-power bolted busbar connections. In: Proceedings of the 11th WSEAS International Conference on Circuits, Greece, pp. 228–233.